Heliyon

Received:
10 November 2018
Revised:
30 January 2019
Accepted:
26 February 2019

Cite as: U. Pramod Kumar, S. Shanmugan, C. Joseph Kennady, S. M. A. Shibli. Anti-corrosion and microstructural properties of Ni−W alloy coatings: effect of 3,4-Dihydroxybenzaldehyde. Heliyon 5 (2019) e01288. doi: 10.1016/j.heliyon.2019.e01288

Anti-corrosion and microstructural properties of Ni−W alloy coatings: effect of 3,4-Dihydroxybenzaldehyde

U. Pramod Kumar [a,d,*], **S. Shanmugan** [a], **C. Joseph Kennady** [b], **S. M. A. Shibli** [c]

[a] *Department of Chemistry, SRM Institute of Science and Technology, Kattankulathur Campus, Chennai, 603203, Tamil Nadu, India*

[b] *Department of Chemistry, Karunya Institute of Technology and Sciences, Karunya Nagar, Coimbatore, 641114, Tamil Nadu, India*

[c] *Department of Chemistry, Kerala University, Karyavattom Campus, Trivandrum, 695, Kerala, India*

[d] *School of Materials Science and Engineering, Jiangxi University of Science and Technology, 156 Hakka Road, Ganzhou, 341000, PR China*

[*] Corresponding author.

E-mail address: pramod7147@gmail.com (U. Pramod Kumar).

Abstract

In the present work impact of 3,4-Dihydroxybenzaldehyde on the microstructural and corrosion behavior of nanocrystalline Ni-W alloy coatings has been elucidated. A systematic investigation on the protection ability of Ni-W alloy coatings in 0.2 M H_2SO_4 solution was done with the aid of tafel polarization curves and electrochemical impedance spectroscopy (EIS) studies. Corrosion performance of the alloy films obtained in the absence and in the presence of different concentrations of 3,4-Dihydroxybenzaldehyde (0−500 ppm) in the bath was explained in the light of additive concentration. Compared to the blank and other concentrations of additive, 250 ppm of additive containing bath was predicted as the most promising one for the introduced citrate based Ni-W alloy electrodeposition. Low corrosion rate (0.06 mm/year) and high charge transfer resistance (2505.3 Ω cm^2), for the electrodeposits, obtained from the bath containing 250 ppm of 3,4-Dihydroxybenzaldehyde supports for its high anticorrosion performance. The marked difference in the corrosion resistance

https://doi.org/10.1016/j.heliyon.2019.e01288

property is ascribed to the formation of fine-grained deposits, smooth surface, and inclusion or adsorption of additive within the deposits in the presence of the additive (250 ppm) in the bath. Further, the adsorption of additive molecules on the metal surface was explored with the help of quantum chemical calculations based on DFT.

Keywords: Materials chemistry, Electrochemistry

1. Introduction

The protection of industrial materials from corrosion process is of paramount importance, not only maximizing the durability of the appliances but also diminishing the toxic metals solubility from the industrial materials into the environment [1]. The demand for increasing the longevity of alloy metals is increasing drastically, due to its wide applications in various fields and in engineering advancements [2]. In comparison with the conventional coatings, reinforced composite possess higher hardness, improved corrosion and wear resistance and dense homogenous electrodeposits with lesser surface roughness. Examples of such reinforcing agents include ceramics, organic materials and metals [3] to name a few. Hexavalent chromium is frequently employed on the relevance of functional mechanical parts due to its good glossy nature, high hardness, and low-cost characteristics [4]. It has become an unavoidable part of many engineering applications, due to its promising features like low coefficient of friction, superior corrosion resistance and wear resistance and other decorative reasons. Significant interest in the development of nanocrystalline Ni-W alloy as surface coatings is receiving considerable attention, since its potential applications are in multiple [5]. This alloy system has become an ideal choice in the industrial sector, owing to its remarkable properties like noticeable corrosion resistance [6], better electrocatalytic property [7] combination of desired hardness and wear resistance [8], stability at higher temperatures [9] and as a effective barrier in electronic/electrical components [10], and moreover this alloy coatings were nominated as a propitious and challenging alternative to the hazardous hard chrome plating [11, 12]. The beneficial exploit of Ni−W alloys to the materials which require resistant to the relatively high temperatures, includes micro and nano-electromechanical systems, sliding contacts or high-temperature superconductors [13, 14]. Despite advances in the fabrication of metallic surface coatings, an electrodeposition method offers a tailored surface property which includes corrosion, wear and fatigue. These are the key components in increasing the lifetime of the tools and components [15]. These tailored surface properties can be attained by altering the electrochemical parameters like pH, temperature, current density and agitation rate which are of prevailing factors. The merits of this process include controlled fabrication of metallic coatings, easily feasible, the ability of continuous processing and reduced waste

https://doi.org/10.1016/j.heliyon.2019.e01288

materials [16]. However, most of the other methods suffer from the disadvantages of requirement of expensive materials and equipments and its complex process limits their application in practical.

An electrochemical reaction occurring in between a metal and its environment i.e. corrosion is costing us a more than 4 trillion dollars per year globally [17]. Detrimental effects of corrosion lead to serious damage to industrial parts and materials which tends to decrease in operating efficiency and cease of production rarely. Slow down or lowering the corrosion rate by surface modification has given a paramount importance than in altering the bulk of material properties [18]. In the light of surface modification, numerous methods came into existence to fight against corrosion phenomenon. Likewise the usage of organic additives or inhibitors in the plating bath or in the corrosive solutions is in practice for several years in the area of corrosion science. Their advantages include multiple adsorption sites, presence of π electrons and moreover stronger adsorption and greater coverage on the metallic surface. It is interesting to note the possibility of interaction between π electrons of the double bond and d-orbitals of the metal which provides a physical insight into the actual reactivity of additives in impeding the corrosion process [1]. Density functional theory (DFT) has become an active field of research, to envisage the mechanism arising between organic additives and surface of the metal at the molecular level [19, 20, 21].

To emphasis, 3,4-Dihydroxybenzaldehyde paved a way as an inhibitor and as an additive that quench the demands of fundamental research and as well as industrial surface engineering components. As an inhibitor [22], have shown that the inhibition efficiency on mild steel in hydrochloric acid increases with the decrease in temperature. Further [23], studied the synergic inhibition effect of rare earth Ce (IV) ion and 3,4-dihydroxybenzaldehye on the corrosion of cold rolled steel in H_2SO_4 solution. The effect of 3,4-Dihydroxybenzaldehyde as an additive on Ni-W electrodeposition remains unknown, so the investigations on these areas of research are the foremost report in the literature.

2. Experimental

2.1. Materials and its function

Nickel sulfate ($NiSO_4.6H_2O$) and ammonium chloride (NH_4Cl) were procured from Fischer Scientific Company which functions as nickel source and as buffer. The rest of the chemicals: sodium tungstate ($Na_2WO_4.2H_2O$), trisodium citrate ($C_6H_5Na_3O_7.2H_2O$), and sodium chloride (NaCl) were purchased from the Merck company, which aids as an source of tungsten, complexing agent, and as an conductor to increase the conductivity of the electrolyte. A 3,4-

https://doi.org/10.1016/j.heliyon.2019.e01288

Dihydroxybenzaldehyde which acts as an additive in the present study was purchased from the sigma Aldrich company. All of the chemical reagents were of analytical (A.R) grade; which were employed as received. The detailed chemical composition and the adopted parameters during electrochemical deposition of Ni-W alloy coatings were formulated in Table 1.

2.2. Fabrication of alloy surfaces

A two electrode system containing Platinized Titanium (25 mm × 25 mm × 1.5 mm) as anode and mild steel as cathode (25 mm × 25 mm × 0.3 mm) were implemented for the electrochemical deposition of Ni-W alloy coatings. Throughout the course of all set of experiments a constant current density of 5 A/dm^2 at 60 °C for 15 minutes was perpetuated. A freshly prepared aqueous sulfate-citrate electrolyte is used for each set of experiments, maintained at pH-8, since electroactive citrate Ni(II) and W(VI) complexes of $[NiC_6H_5O_7]^-$ and $[(WO_4)\ (C_6H_5O_7)\ (H)]^{4-}$ types occur at a significant concentration. The bath used for the present study was used as the source reported elsewhere [24]. Prior to each plating, the cathodic substrates were degreased with acetone in ultrasounds to remove loosely adsorbed contaminants on the surface. Further, it was electrochemically polished in an alkaline solution of NaOH (3.5 g/l) and Na_2CO_3 (2.5 g/l) at ambient temperatures in-order to detach the surface passive oxide film effectively. Right in earlier to the plating the steel substrates were activated in 10% H_2SO_4 solution for 30–40 seconds and then transferred to the plating bath instantly. An immense care has been taken during the pretreatment process, as it shows marked effect on the adhesion of coating on the substrate [25]. Succeeding, the substrates were given a water wash followed by hot blow in order to remove loosely adsorbed particles/rudimental solutions from the coating surface. For being confident of the reproducibility; experiments were reiterated in order to optimize the concentration of the additive in the electrodeposition bath. The current efficiency of the alloy was calculated based on the faradays law as

Table 1. The electrolyte composition and parameters used for electrodeposition of Ni-W alloy coatings.

Bath constituents	Concentration (M)	Operating conditions
$NiSO_4.6H_2O$	0.1	Temperature 333 ± 3 K
$Na_2WO_4.2H_2O$	0.2	Current density 5 A dm^{-2}
$C_6H_5Na_3O_7.2H_2O$	0.5	pH 8
NaCl	0.1	Deposition time 15 min
NH_4Cl	0.5	Anode- platinized titanium
$C_7H_6O_3$	0–500 ppm	Cathode- mild steel

https://doi.org/10.1016/j.heliyon.2019.e01288

$$\eta_c = \frac{W_1}{W_2} \times 100 \quad (1)$$

where W_1 is the weight deposited in g and W_2 is the weight expected in g:

$$W_2 = \frac{ItM}{nF} \quad (2)$$

where I is the current in A, t the time in s, M the molecular weight in g, n the number of electrons involved in the electrochemical reaction, and F is the Faraday's constant F = 96,500 As.

To minimize the error, the average of 10 measurements performed at different areas of sample was taken as final value of deposit thickness, measured by means of METRAVI (CTG-01) digital coating thickness tester. The X-ray diffraction characterization was conducted using Shimadzu XRD 6000 (Japan) instrument equipped with a Cu-Kα radiation source. Patterns were used to determine phase structure and an average crystallite size of the alloy deposits was calculated using Scherrer formulae [26]. Morphological analysis of the Ni−W coatings acquired of as such and the optimized one was complemented by scanning electron microscopy (JSM-360; JEOL) and composition analysis using the same detector (SEM-EDS) on the SEM. Atomic force microscopy (AFM) (Bruker-dimension icon AFM equipped with a Scan Asyst) was used to know the maximum surface roughness (Rmax) of the alloy deposits at atomic resolution respectively. The adsorption of additive molecules on the surface of the alloy was determined using Photoluminescence (PL) JASCO model FP-8200 system. The incorporation of additive in the deposits during electrodeposition was achieved by using Fourier transform infrared spectroscopy (IR Prestige-21 Shimadzu, Japan).

Corrosion resistance evaluation of Ni-W coatings, both in as plated and with various concentrations of additive (0−500 ppm) in the plating bath were performed using potentiodynamic polarization and electrochemical impedance spectroscopy (EIS) studies using a potentiostat/galvanostat instrument (CHI660C computer-controlled potentiostat/galvanostat (USA) in 0.2 M H_2SO_4 solution at room temperature. A three-electrode cell assembly was employed for the measurements. The electrodeposited alloy coatings with an exposed area of 0.2 cm^2 served as working electrodes (WE), while the undesirable parts of the substrate were masked with lacquer. Platinum foil with a larger area was used as the counter electrode (CE) and a saturated calomel electrode (SCE) was used as the reference electrodes (RE). Both of the measurements were performed at their respective open circuit potentials (OCP). Impedance measurements were carried out at open circuit potential of the working electrode by applying a 5 mV AC sine wave perturbation over a frequency range of 1 Hz−100 kHz. Impedance measurements were represented in the form of Nyquist plots. The equivalent circuit simulation program, Z-view (3.0 version) was used for the fitment of the equivalent circuit and data analysis. For potentiodynamic

https://doi.org/10.1016/j.heliyon.2019.e01288

polarization studies, the electrode potential was fixed at the open circuit potential (OCP), and the steady-state polarization was carried out from ±200 mV to the OCP at a scan rate of 10 mV s^{-1}. The corrosion potential (E_{corr}) and corrosion current density (i_{corr}) were intended using Tafel extrapolation method from the obtained polarization results [27]. In order to obtain the reproducible data, the measurements were repeated twice under same conditions. The protection efficiencies (P.E) were deliberated from the obtained corrosion current and charge transfer resistance values, using the equations that reported elsewhere [28]. The degree of surface coverage (Θ) was calculated using the following equation

$$\theta = \frac{i_o corr - i_{corr}}{i_o corr} \tag{3}$$

All the quantum related calculations were carried out by density functional theory (DFT) using the B3LYP functional method with electron basis set 6-311G (d,p) for all atoms of the studied system. The quantum chemical calculations under investigation were done by the Gaussian 09 program package at 333 K with water as a solvent in the IEFPCM theoretical model. The following quantum related parameters were considered in main: the energy of the highest occupied molecular orbital (E_{HOMO}), the energy of the lowest unoccupied molecular orbital (E_{LUMO}), energy band gap $\Delta E = E_{LUMO} - E_{HOMO}$ and Mulliken charges of all atoms.

3. Results and discussion

3.1. Electrochemical evaluations

Tafel polarization technique was employed to obtain the corrosion kinetic parameters of corrosion process for Ni-W coatings obtained at various concentrations (0−500 ppm) in the plating bath (Fig. 1) that overt the corrosion behavior of coating system. The obtained parameters from the Tafel plots are tabulated in Table 2. As evidenced from Fig. 1 and Table 2, the alloy deposits acquired from the bath, containing 250 ppm of 3,4-Dihydroxybenzaldehyde have the noblest of corrosion potentials among the considered coatings. The primary impediment in nickel and its alloy plating baths is the formation of structural defects like crevices, gaps and porosities formed due to the hydrogen evolution near the cathode [29, 30]. The adsorption or inclusion of additive into the surface heterogeneities (small holes and porosities) of Ni-W alloy coatings, helped in the reduction of ion diffusion process in the presence of a corrosive medium. In consideration of the corrosion current density (i_{corr}), it was initially decreased and then increased as the additive concentration increased beyond 250 ppm in the bath. The decrease in the corrosion current resulted in lower corrosion rate (0.06 mm/year), which alludes that a thin dense passive film has been formed separating the electrode from corrosion species and therefore reducing the chances for the formation of high energy defective regions (or) active

https://doi.org/10.1016/j.heliyon.2019.e01288

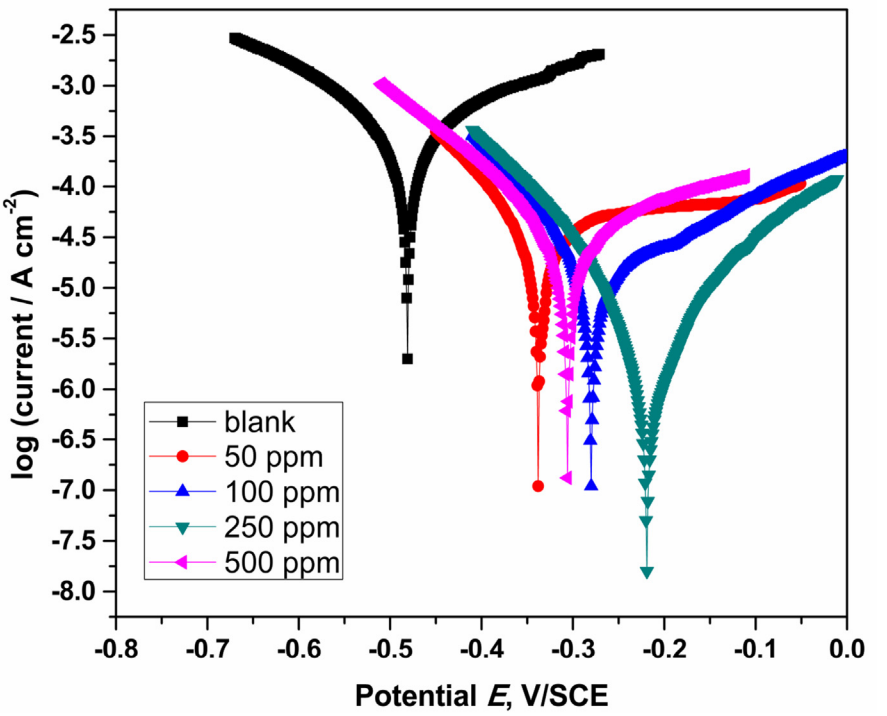

Fig. 1. Potentiodynamic plots of Ni-W alloy coatings of as deposited and at various concentrations (50−500ppm) of 3,4-Dihydroxybenzaldehyde in the plating bath.

sites. Among the considered coatings, the electrodeposits obtained in the presence of 250 ppm of additive, displays the greater polarization resistance value of 14902.6 Ω cm^2 which explicit the sterling adsorption capacity of an added additive of alloy coating onto the mild steel, consequently resulting in the good protection efficiency (99.66%). The degree of surface coverage gives the information about the contact area between the additive molecule and metal surface [31]. Higher surface coverage value of $\Theta = 0.99$ is seen in the case of alloy deposits obtained from the optimized bath (250 ppm), which is proportional to the increase in adsorptive property and in the protection efficiency. In conclusion, tafel results imply that the alloy coatings obtained from the bath containing 250 ppm of additive, revealed a decreased oxidation tendency of the alloy metal obtained on the mild steel that substantiates its firm adhering property.

EIS is one of the prevailing analytical techniques, which gives information about interfacial interactions of the test specimen, through popularly called Nyquist diagram [32]. Accordingly, the Nyquist response of Ni-W alloy coatings obtained without and with additive at varied concentration in the bath was plotted as imaginary impedance vs real impedance and represented in Fig. 2. The inset provides a simulated electrochemical equivalent (ECE) circuit obtained with the aid of Z-View software (version 3.0). Here Rs = solution resistance, Rct = charge transfer

https://doi.org/10.1016/j.heliyon.2019.e01288

Table 2. Significant data obtained from the tafel polarization curves for Ni-W alloy coatings of as deposited and with that of 3,4-Dihydroxybenzaldehyde at varied concentration (0−500 ppm).

Concentration of 3,4-Dihydroxybenzaldehyde (ppm)	E_{corr} (mV vs SCE)	i_{corr} (μA/cm^2)	Θ	PE (%)	CR (mm/year)	R_p (Ω cm^2)
0	−481	434.0	—	————	17.90	100
50	−338	41.22	0.90	90.50	1.77	899.1
100	−280	13.34	0.96	96.92	0.57	1923.4
250	−219	1.463	0.99	99.66	0.06	14902.6
500	−306	35.48	0.91	91.82	1.53	1062.3

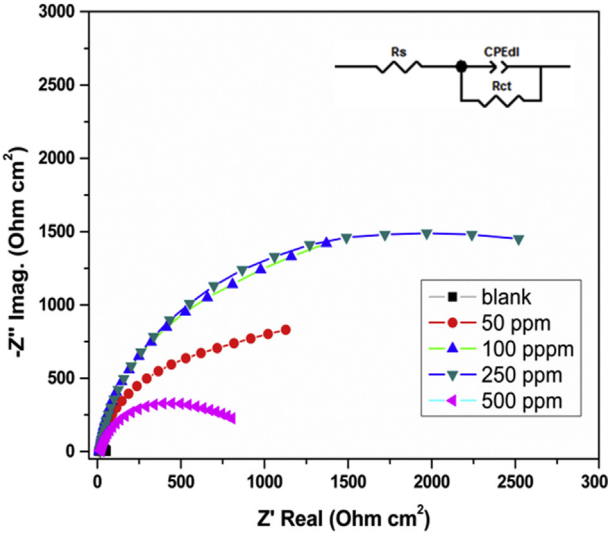

Fig. 2. EIS measurements represented with Nyquist curves of Ni-W alloy coatings of as deposited and for deposits obtained from the bath containing 50, 100, 250, 500 ppm of additive. Inset provides the equivalent electrical circuit (R_s = Solution resistance, R_{ct} = Charge transfer resistance and CPE_{dl} = Constant phase element).

resistance and CPE_{dl} = constant phase element as a substitution for double layer capacitance (C_{dl}). Typically C_{dl} acts as constant phase element (CPE) rather than a pure capacitor, which accounts for deviation from ideal dielectric behavior related surface inhomogeneities [33]. The CPE characterizes, the deviation of ideal capacitive behavior, where n = 1 (ideal capacitor) and n = 0 (ideal resistor). The results obtained from the fitment of semicircles and the calculated surface roughness factor (Rf) values are tabulated in Table 3. The diameter of the semicircle is considered as charge transfer resistance. From Fig. 2 it can be observed that all the alloy coatings exhibited a Nyquist response with an incomplete depressed semicircle, which attributes to the surface roughness and inhomogeneity of metal surface which is typical for solid metal electrodes [34]. However, the identical shapes of Nyquist plots

https://doi.org/10.1016/j.heliyon.2019.e01288

Table 3. Summary of significant data procured from the EIS measurements for the Ni-W alloy coatings of as deposited and with that of 3,4-Dihydroxybenzaldehyde at varied concentration (0−500 ppm).

Concentration of 3,4-Dihydroxybenzaldehyde (ppm)	R_s (Ω cm^2)	C_{dl} (μFcm^{-2})	R_{ct} (Ω cm^2)	PE (%)	Rf	n
0	6.40	85.70	49.50	———	4.285	0.81
50	10.78	53.66	1116.4	95.5	2.683	0.90
100	11.23	50.88	1360.0	96.3	2.544	0.92
250	18.18	25.64	2505.3	98.0	1.282	0.94
500	22.46	43.55	789.3	93.7	2.1775	0.88

indicate that corrosive medium was unable to reach the substrate (mild steel) through the alloy coating and corrosion mechanism of the coating is constant [30]. A clear demarcation, i.e. increase in axial radius (Rct = 2505.3 Ω cm^2) of the semicircle is seen in Ni-W alloy coatings (250 ppm) which notifies the improved corrosion resistance property. Rct values give a quantity of electron transfer across the surface, which is inversely proportional to the rate of corrosion [35]. The obtained Rct values (Table 3) are in compliance with the corrosion rate values derived from tafel curves (Table 2). A lower C_{dl} value (25.64 μFcm^{-2}) and higher n value (0.94) for the alloy coatings electrodeposited by 250 ppm of additive from the bath are an indicative of better surface homogeneity with higher capacitive nature, consequent to the lesser amount of current flow through it [32]. Based on the obtained C_{dl} values, a surface roughness (Rf) of the Ni-W alloy coatings were estimated from the proportion of double layer capacitance of the coatings, C_{dl} to that of the smooth electrode was considered as 20 μFcm^{-2} [36]. In addition to this, a low Rf value (1.28) assents to the above results, ascertaining that the alloy deposits obtained by 250 ppm of additive from the bath are the most corrosive resistant and the optimal one among the studied concentrations. However, at other concentrations the decline in Rct and increase in C_{dl} is observed; suggesting that film protection aggravate by adding too much of 3,4-Dihydroxybenzaldehyde in the plating bath. In fact, above some critical concentration, the presence of organic compound in a plating bath will bind to particular areas of the alloy deposits; subsequently become trapped in the deposit or cause the significant amount of hydrogen gas evolution, thus increasing the probability for the formation of gas pits [37]. Moreover, lower n values and higher C_{dl} values (Table 3) indicate its poorer capacitive nature due to cracks or pores [38]. The schematic illustration of adsorption of additive molecules onto the surface of alloy is shown in Fig. 3. A similar trend in protection efficiency is observed for the results obtained from the EIS and tafel measurements.

Further, in our investigation, the corrosion resistance property of Ni-W alloy coatings arises owing to the interplay between surface morphology and its roughness.

https://doi.org/10.1016/j.heliyon.2019.e01288

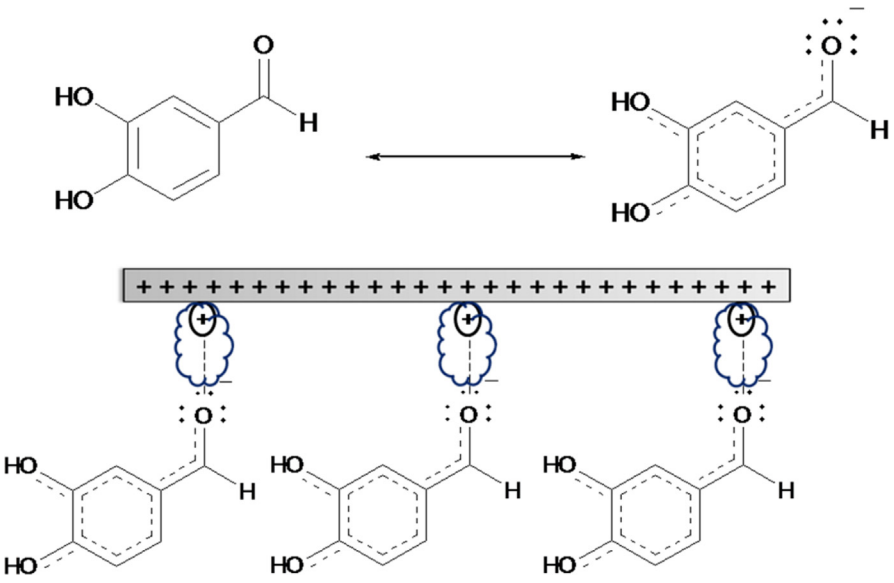

Fig. 3. Schematic illustration of additive adsorption onto the alloy surface.

So in order to process, the optimized and the blank one are examined further using XRD, SEM-EDAX, AFM and other surface characterization techniques.

3.2. Crystallization analysis

Fig. 4 (a-b) was the X-ray diffraction patterns of Ni-W alloy deposits obtained of as such and with that of 3,4-Dihydroxybenzaldehyde (250 ppm) in the bath. The appearance of peaks from the X-ray diffraction patterns at 2θ angles of 43.5°, 66.0°, corresponds to Ni-W peaks with a body centered cubic structures (JCPDS cards. no.65−2673). The corresponding planes of (211) and (400) suggests the existence of $Ni_{17}W_3$ phase. The average crystalline size of nanocrystalline Ni-W alloy deposits was calculated using Debye scherrer equation, based on full width at half maximum (FWHM). Based on the calculations, the crystalline size of the Ni-W alloy deposits estimated to be 12 nm for the earlier one (Fig. 4.a) and 3.0 nm for the former one (Fig. 4.b). The alloy electrodeposits produced with the aid of 250 ppm of 3,4-Dihydroxybenzaldehyde in the bath, resulted in a smaller crystalline size, consequently showed a greater resistance towards localized corrosion, which attributes to the even distribution of corrosion current [39]. The decrease in the intensity of diffraction peaks and peak width broadening of Ni-W coatings (Fig. 4(b)) corroborates the reduction in grain size, demonstrating the role of added additive as grain refiner. In conclusion, XRD result suggests that the adsorption of additive during crystal growth has increased the competition between nucleation and growth, leading to increasing in nucleation rate, which eventually resulted in smaller crystalline size [30].

https://doi.org/10.1016/j.heliyon.2019.e01288

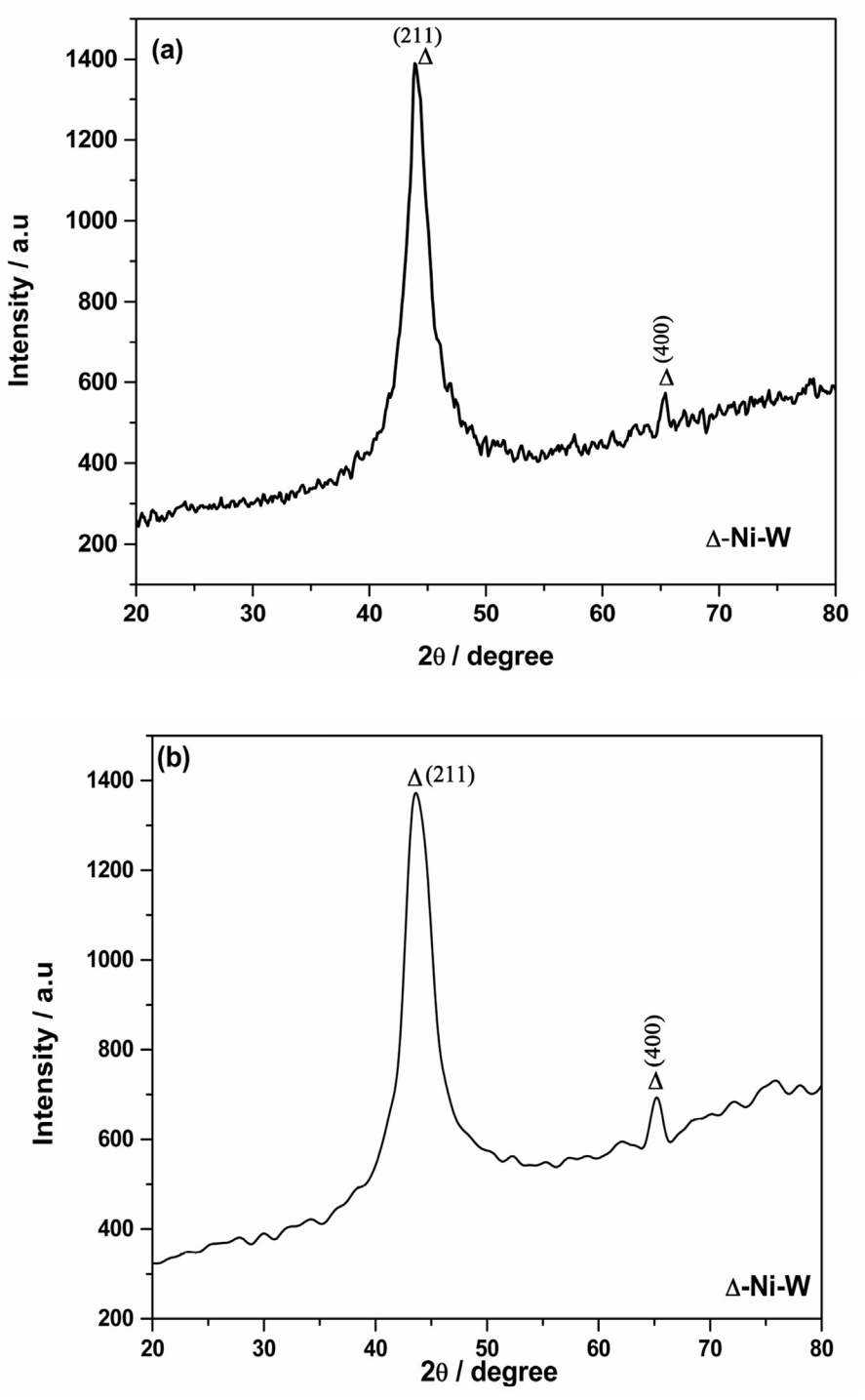

Fig. 4. X-ray diffraction data for Ni-W alloy coatings of as deposited and with that of 3,4-Dihydroxybenzaldehyde (250 ppm) in the plating bath.

https://doi.org/10.1016/j.heliyon.2019.e01288

3.3. Microstructural characteristics

Optical images of Ni-W alloy coatings obtained of as such and in presence of an additive (250 ppm) from the citrate baths are shown in Fig. 5 (a-b). It is evident from the optical images, that as such Ni-W alloy deposits (Fig. 5(a)) were coarse-grained irregular, and random distribution of dissimilar grains exhibiting uneven surface whereas, the Ni-W deposits (Fig. 5(b)) obtained from the bath containing (250 ppm of 3,4-Dihydroxybenzaldehyde) was regular and smoother through fine grains, revealing even surface morphology. This study proves that added additive helped in yielding compact and homogeneous deposit.

Surface morphology of Ni-W alloy coatings obtained from the bath in the absence and presence of the additive (250 ppm) examined by SEM is illustrated in Fig. 6 (a-b). The surface morphology of as such (Fig. 6(a)) exhibits a non-uniform surface structure with loose morphologies exhibiting larger micropores or micro cracks which is the cause for the accelerated dissolution of alloy coatings in the corrosive medium. The general admitted mechanism for the micropores is the hydrogen evolution at the cathode surface [40]. Whereas the deposit obtained in the presence of an additive (250 ppm) resulted in uniform surface structure with well defined facets and compact deposits with few spheroids, suggesting that the added additive helped in reducing crystal growth, by enhancing the number of nucleation sites during electrodeposition, ultimately contributing to an enhancement in the nanocrystalinity of the alloy deposits [41]. Compositional data collected using EDAX for the alloy deposits of as such and in the presence of an additive (250 ppm), were displayed in inset of above figures. The obtained graphs portray that nickel content increased from 53.23 wt% to 60.32 wt% of the alloy coatings, electrodeposited in the presence of the additive. However, tungsten content decreased from 46.77 wt% to 39.68 wt% of the alloy coatings, electrodeposited in the presence of the additive in the bath. In generic, composition of alloys primarily depends on the ionic mobility and ionic concentration at the cathode solution interface. Those factors depend on the parameters like current density, temperature, agitation, bulk metal ion concentration and mass of the ions (metal/non-metal) [42]. Several studies have reported that Ni^{+2}- citrate complex has faster ionic mobility than W-citrate complex [43]. Here in our study also the same trend is seen. Therefore it hypothesized that the added additive has decreased the surface concentration of citrate-tungsten complex, which resulted in the less amount of tungsten percentage (39.68 wt %), that eventually raised the amount of nickel percentage (60.32 wt%) [44]. Table 4 summarizes the relation of current efficiency and thickness with the tungsten percentage. For citrate based metal tungstate alloys ($NiWO_4$) the dominant phase is a solid solution of W in nickel [45].

The average thickness of alloy coatings deposited in the absence (0 ppm) and in the presence of additive (250 ppm) in the bath is found to be 20.5 μm and 17.0 μm respectively. A thinner coating with more surface coverage ($\Theta = 0.99$) was obtained

https://doi.org/10.1016/j.heliyon.2019.e01288

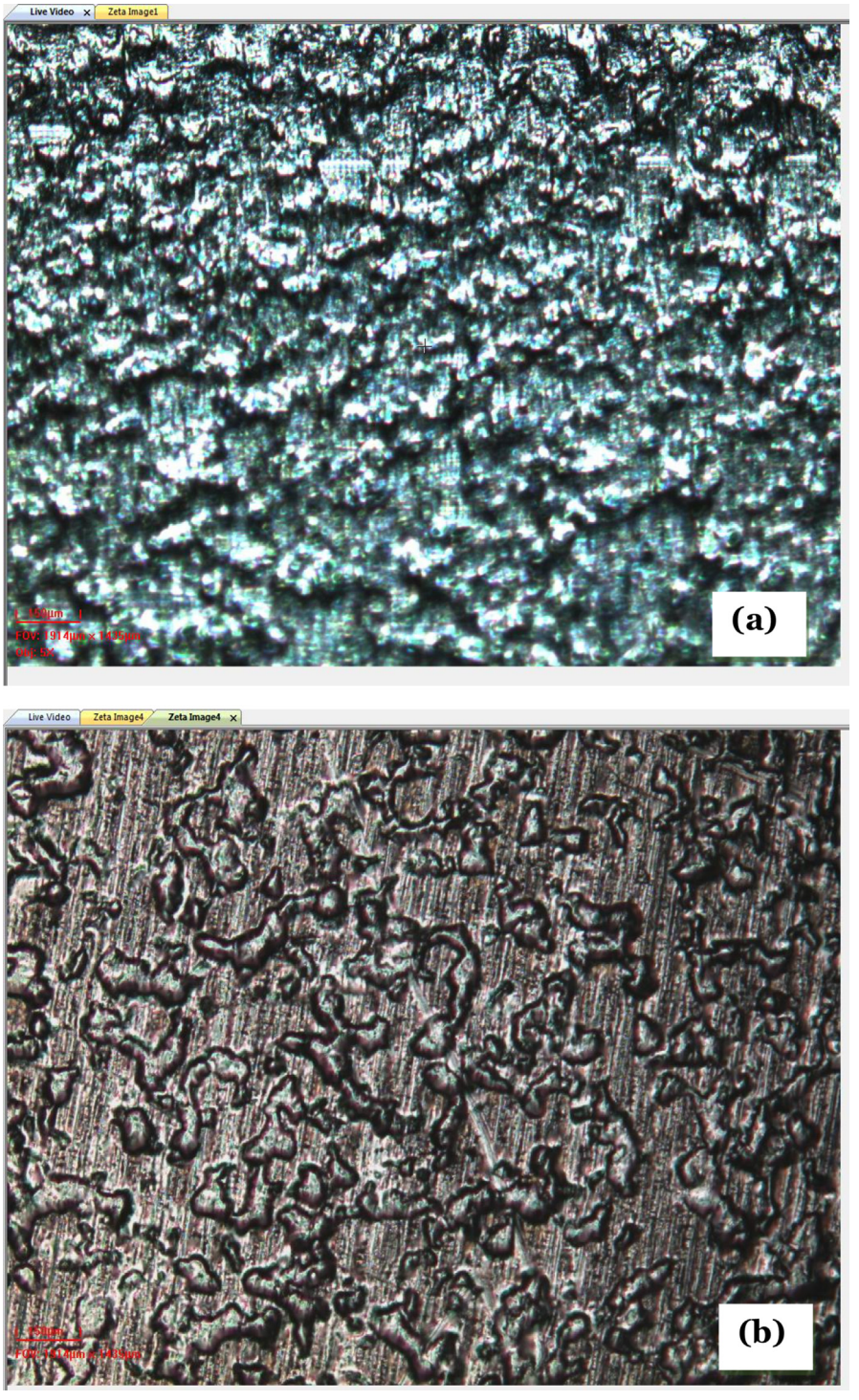

Fig. 5. Optical images of alloy coatings (a) of as deposited (b) with that of 3,4-Dihydroxybenzaldehyde (250 ppm) in the electrolytic solution.

https://doi.org/10.1016/j.heliyon.2019.e01288

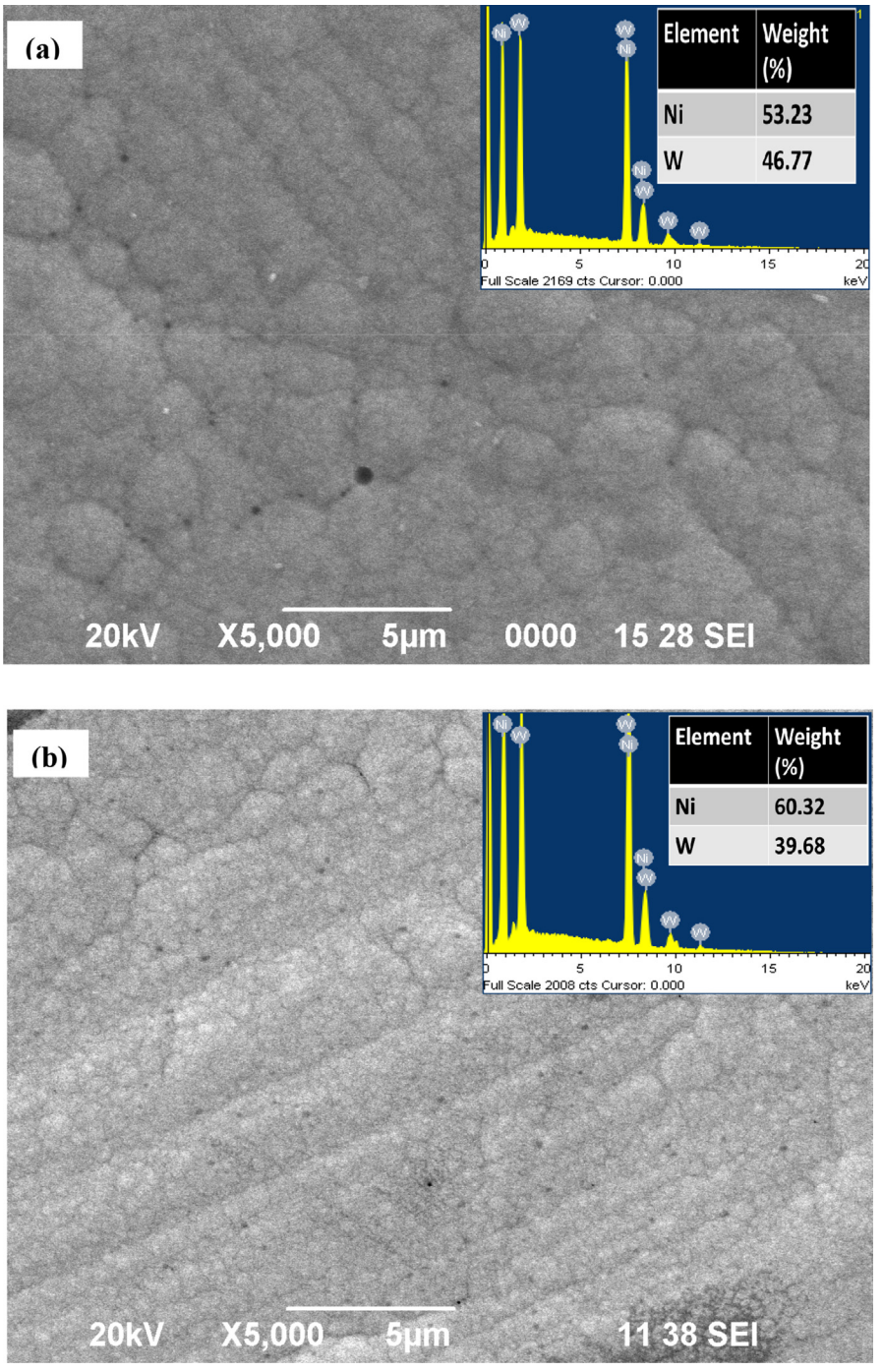

Fig. 6. Surface morphology/compositional data of Ni-W coatings obtained from the plating baths (a) 0 ppm (b) 250 ppm of 3,4-Dihydroxybenzaldehyde.

in the presence of additive (250 ppm) in the bath, which implies a uniform and smoother coating. Even so, the decrease in thickness may be influenced by the additives in the bath through a water side reaction [46]. The current efficiency is found to be higher (51%) in the case of alloy deposits with lower tungsten (39.68 wt%) and

https://doi.org/10.1016/j.heliyon.2019.e01288

Table 4. Effect of Tungsten wt% on CE and thickness of the electrodeposits.

Tungsten Wt%	Thickness (μm)	CE (%)
46.77	20.5	45
39.68	17	51

for higher tungsten percentage it was of lower current efficiency (45%) (Table 4). The possible reason for lower current efficiency is the hydrogen side reaction at the cathode surface [47]. Nonetheless, in our earlier reports, we proved that corrosion resistance property of Ni-W alloy coatings depends on the kind of additive molecules adopted in the plating baths, despite tungsten percentage [48].

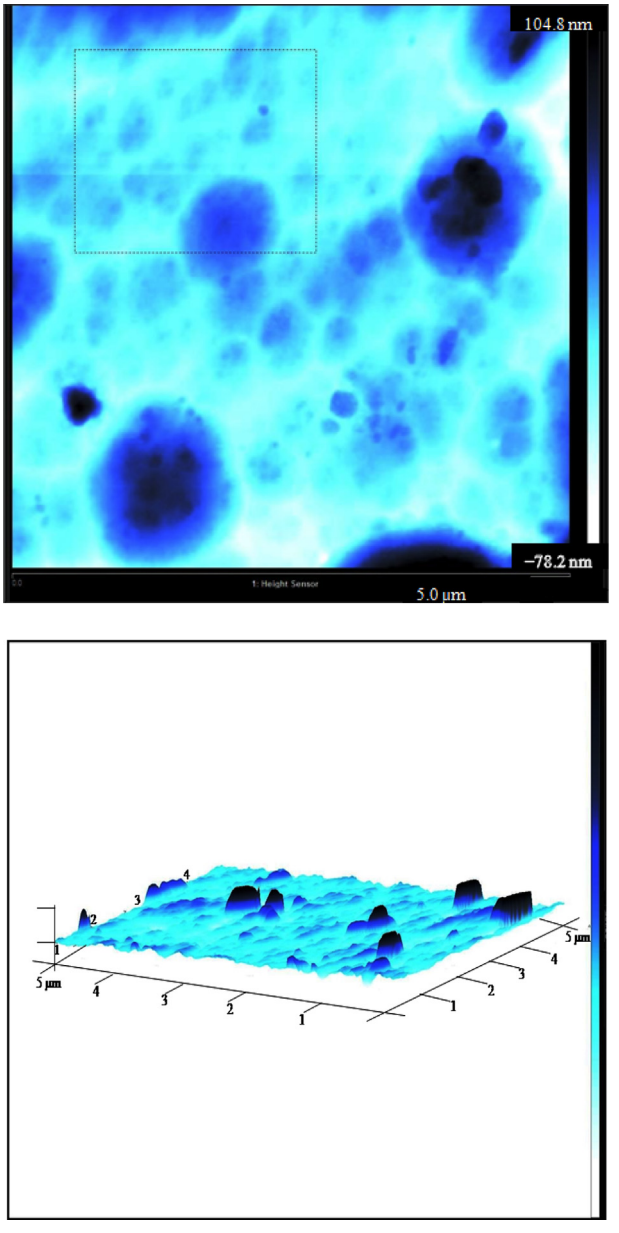

Fig. 7. 2D and 3D AFM images of Ni-W alloy electrodeposits.

https://doi.org/10.1016/j.heliyon.2019.e01288

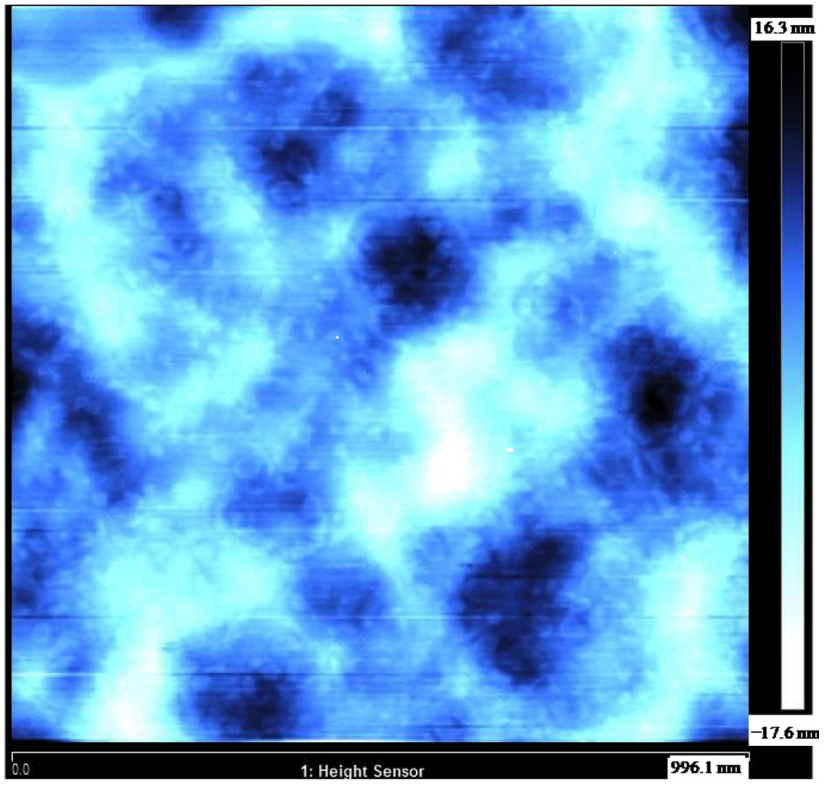

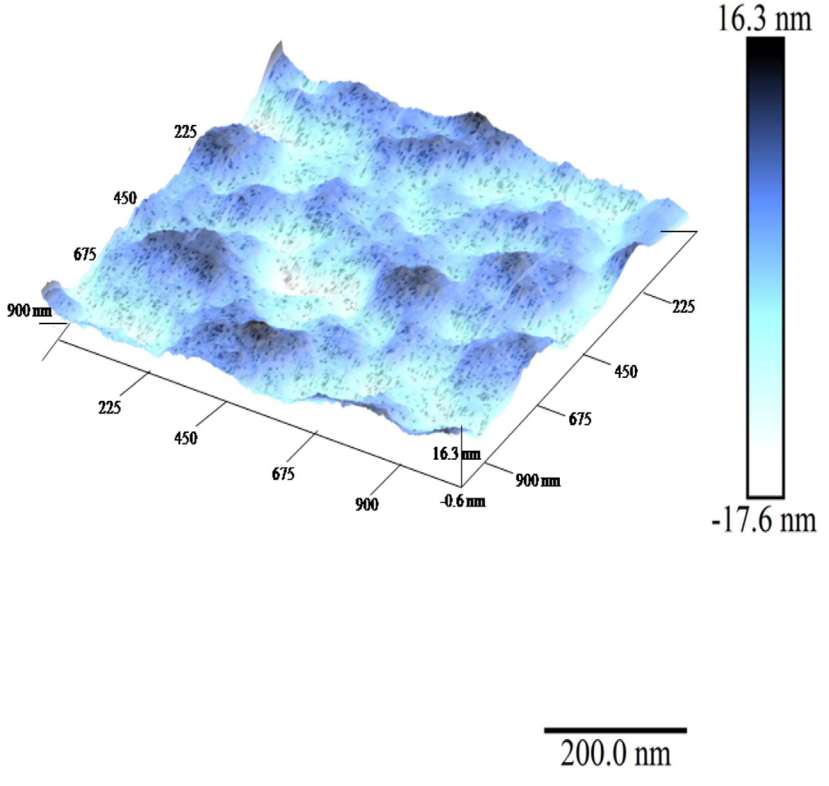

Fig. 8. 2D and 3D AFM images of Ni-W alloy electrodeposits obtained from the bath containing 3,4-Dihydroxybenzaldehyde (250 ppm).

https://doi.org/10.1016/j.heliyon.2019.e01288

Further, for a precious investigation on the surface morphology, surface roughness analyzed using AFM is taken into consideration for the alloys electrodeposited as such and in the presence of an additive (250 ppm) in the bath. These experimental results show that surface roughness (R_{max}) of Ni-W alloy deposited in the presence of an additive (250 ppm) showed a decrease in the R_{max} value (30.0 nm) when compared with that of blank one (72.5 nm). The 2D and 3D topographic images of Ni-W coatings shown in Figs. 7 and 8 witnesses for the results above mentioned. The higher surface roughness and irregularities in the former one are observed owing to the nature of kinetics and mass transfer during electrodeposition [49]. In contrast, the electrodeposits obtained from the additive induced bath, resulted in smoother and glossy surface with a reduction in surface roughness by detracting the metal ions from sharp protuberances [50, 51, 52]. Further, the reduction in the R_{max} value infers that added 3,4-Dihydroxybenzaldehyde helped in increasing the nucleating rate and lower growth speed, which eventually resulted in the uniform surface deposition, consequently higher corrosion resistance towards corrosion attack [53]. A smooth surface and compact structures are an indicative of its barrier property i.e. reducing the attack of corrosive medium (SO_4^{2-} ions) from erosion of coating.

3.4. FTIR analysis

Fig. 9 depicts the Infrared spectrum of alloy coatings, electrodeposited from the optimized bath (250 ppm). The spectrum shows absorption peak around 667.37 cm^{-1} is assigned to the aromatic -C-H stretching. The absorption peaks at 1020.34 cm^{-1}

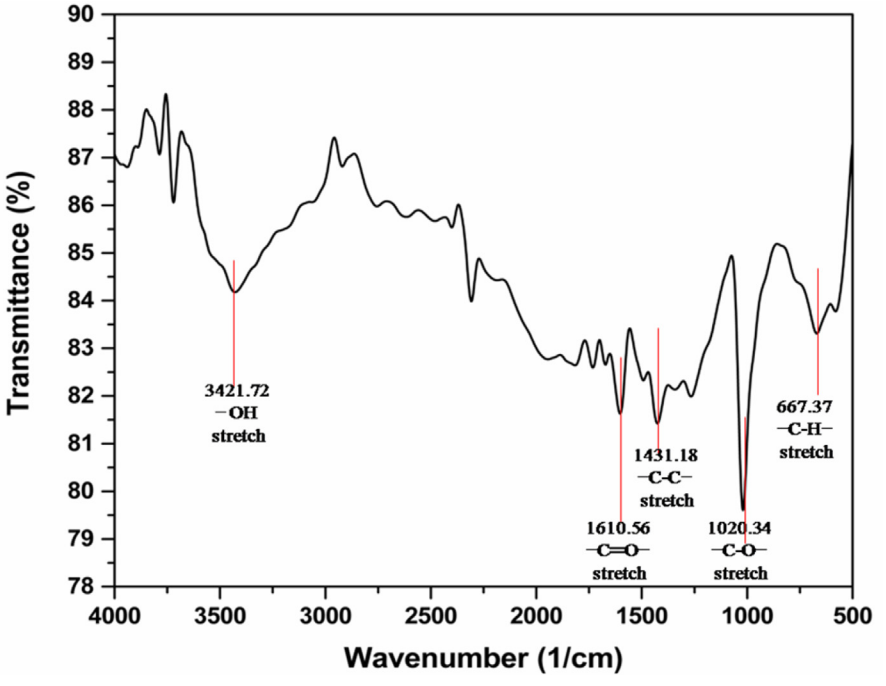

Fig. 9. FTIR spectra of Ni-W alloy electrodeposits deposited from the optimized bath (250 ppm).

https://doi.org/10.1016/j.heliyon.2019.e01288

correspond to −C−O stretching of ring hydroxyl group, the peak at 1431.18 cm^{-1} corresponds to C−C in-ring stretching of the benzene ring. The peak at 1610.56 cm^{-1} is assigned to the C=O stretching and the peak at 3421.72 cm^{-1} corresponds to −OH (hydroxyl) group of addition agent. Thus the obtained absorption peaks in the FTIR spectrum exhibited the incorporation of additive molecules within the pores or layers of the electrodeposits during electrodeposition as demonstrated elsewhere [54]. The findings of this result suggest that added additive acts as pore filler during electrodeposition, which eventually resulted in homogenous deposits.

3.5. PL spectra

Photoluminescence (PL) spectroscopy is one of the versatile characterization techniques for surface of alloy that aid in the analysis of adsorbates on the surface virtually [55]. The adsorption of additive molecules onto the metal surface was further revealed from the photoluminescence measurements. Fig. 10 depicts the PL spectra of Ni-W alloy coatings obtained of as such and in presence of an additive (250 ppm) in the bath respectively. The excitation wavelength (λ_{ex}) was 246.0 nm. A significant increase in intensity of photoluminescence for the sample (Fig. 10.b) implies that there has been a chelation of the aldehyde with the surface of alloy i.e. Chelation enhanced fluorescence (CHEF). The obtained spectra demonstrate that the additive molecules are adsorbed onto the surface of alloy, as illustrated by previous reports [48].

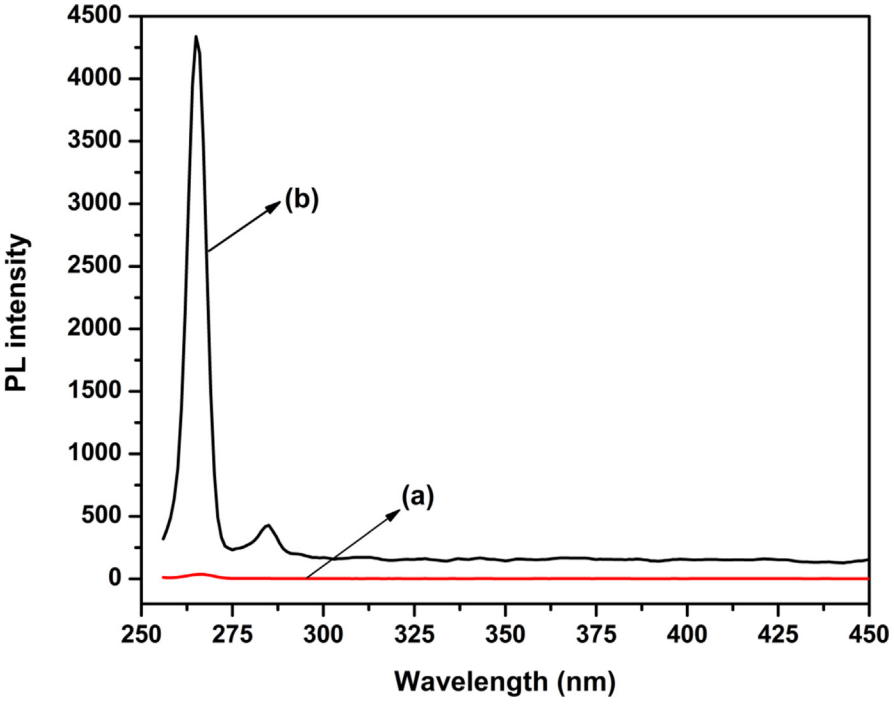

Fig. 10. PL spectra for Ni-W alloys (a) without additive (b) with additive (250 ppm) attained with a xenon flash lamp as source.

https://doi.org/10.1016/j.heliyon.2019.e01288

3.6. Quantum chemical study

In further, to verify the prediction i.e. to prove the additive molecules adsorption on the surface of metal and to compare with the obtained electrochemical results; quantum chemical calculations using DFT principle was employed. The following quantum chemical parameters were extracted from the calculations, which includes highest occupied molecular orbital (E_{HOMO}), lowest unoccupied molecular orbital (E_{LUMO}), energy band gap $\Delta E = E_{LUMO} - E_{HOMO}$. According to frontier molecular orbital theory, the energy of HOMO and LUMO are often correlated with the electron donating and accepting ability of the organic molecules, respectively [56]. In addition, the energy gap (ΔE) is an indicative of interaction between the reactive species [57]. Fig. 11 (a-b) shows the localization of HOMO and LUMO of 3,4-Dihydroxybenzaldehyde. Based on the study of bonding reaction and cloud distributions of organics, these crimson and green color clouds corresponds to the phase of orbital wave functions; in which one is for the negative phase and the other one for the positive phase [56]. The displayed Fig. 11 (a) clearly depicts that HOMO density

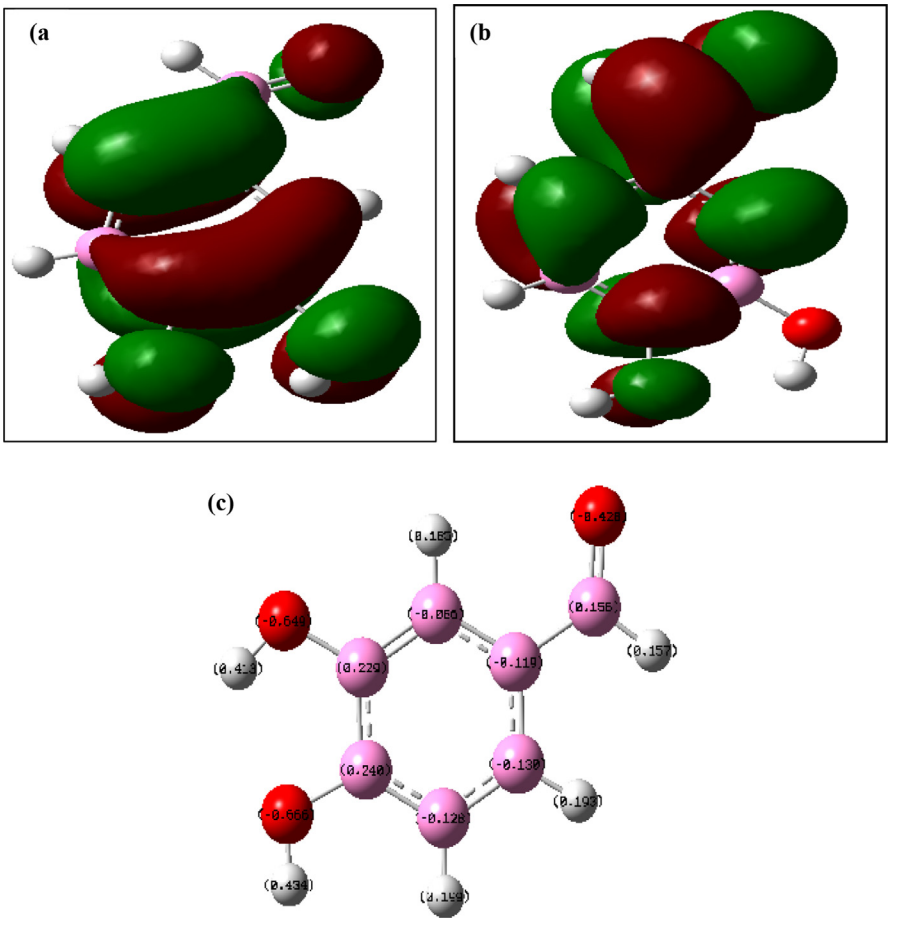

Fig. 11. (a) Localization of HOMO; (b) Localization of LUMO; (c) Mulliken population charge analysis.

https://doi.org/10.1016/j.heliyon.2019.e01288

is largely disseminated in the vicinity of oxygen atoms. A similar distribution of LUMO density (b), is seen in the vicinity of oxygen atoms. These results suggest that oxygen atoms are the favorable sites for the adsorption of an additive on the alloy surface. In generic, oxygen atoms have the property of electron donation, which is associated with its strong adsorption ability on the metal surface.

In addition to the localization of orbitals, quantum chemical parameters obtained from DFT calculation, which describes the adsorption behavior and electronic property of studied additive, are displayed here: $E_{HOMO} = -6.55$ eV and $E_{LUMO} = -2.09$ eV and its $\Delta E = 4.45$ eV. A high value of E_{HOMO} (-6.55 eV) is an indicative of its stronger adsorption capacity, by donating the electrons to the appropriate acceptor molecules with low energy empty molecular orbitals [1]. Further, increased E_{HOMO} value facilitates its effective adsorption on the cathode surface resulting in the enhanced protection efficiency by influencing the charge transfer process throughout the adsorbed organic layer [58, 59, 60]. Similarly, a lower value of E_{LUMO} (-2.09eV) shows a better probability of a molecule to accept the electron [61], which results in the stronger adsorption on the alloy surface. In principle, the adsorption capacity of the organic molecules to the surface of metal increases with an increase of E_{HOMO} or a decrease of E_{LUMO}, this would produce a stronger organic adsorption on the metal surface [53]. In the same way, the smaller energy gap between frontier molecular orbitals ($\Delta E = 4.45$ eV) shows stronger chemisorption bond and greater adsorption stability [58] of the additive molecules on the metal or alloy surface. Moreover, a lower value of energy gap ($\Delta E = 4.45$ eV) indicates the effective adsorption of additives on the surface of metal that depicts the greater electron transfers between the molecular orbits. In addition to this, mulliken population analysis, displayed in Fig. 11 (c) gives mechanistic information of additive adsorption onto the alloy surface. Excess of negative charge is seen in the case of oxygen atoms, then the other atoms. This clearly denotes the electron donating ability of oxygen atom to the unoccupied metal atomic orbitals, which are acting as reactive sites for the effective adsorption.

4. Conclusion

In summary, the results obtained from the electrochemical evaluations exhibited that the presence of 250 ppm of additive in the plating bath produced a highly corrosive resistant Ni-W alloy coatings when compared with the other concentrations (0, 50, 100, 500 ppm). The protection efficiencies determined by tafel polarization and EIS measurements are in good agreement. The alloy deposits obtained from the optimized bath (250 ppm) resulted in a higher surface coverage depicting the good adsorption property resulting in a smooth and compact electrodeposits with smaller crystalline size, which attributes to its remarkable corrosion resistance property. However, the alloy deposits electrodeposited from the bath other than the optimized one

https://doi.org/10.1016/j.heliyon.2019.e01288

showed mediocre corrosive resistance due to the possible surface defects on the coatings surface. The obtained quantum chemical calculations and mulliken population analysis, confirm the adsorption of additive molecules onto the alloy surface through the oxygen atoms and π electrons of the aromatic ring as its active centers. The theoretical and experimental data shows a good relation with each other, which confirms the reliability of DFT principle in studying the additive adsorption. The obtained experimental and theoretical results affirm that a scenario of competitive adsorption of additive molecules onto the alloy surface is the plausible mechanism for corrosion inhibition of Ni-W alloy coatings in sulphuric acid solutions. As there is a massive increase in the environmental pressure to find an alternative for the carcinogenic hexavalent chromium, we deduce that the present study should find wide applicability in the industrial sector as a safer alternative to the hexavalent hard chromium plating.

Declarations

Author contribution statement

U. Pramod Kumar: Conceived and designed the experiments; Performed the experiments; Analyzed and interpreted the data; Wrote the paper.

S. Shanmugan: Contributed reagents, materials, analysis tools or data.

C. Joseph Kennady: Conceived and designed the experiments; Contributed reagents, materials, analysis tools or data.

S.M.A. Shibli: Analyzed and interpreted the data.

Funding statement

The authors would like to thank the Science and Engineering Research Board, Department of Science and Technology, Government of India for the award of National Postdoctoral Fellowship (PDF/2017/002908).

Competing interest statement

The authors declare no conflict of interest.

Additional information

No additional information is available for this paper.

Acknowledgements

The authors acknowledge Prof. Tongxiang Liang, Jiangxi University of Science and Technology, Ganzhou, for the assistance rendered in critically reading the manuscript.

https://doi.org/10.1016/j.heliyon.2019.e01288

References

[1] S. Benabid, T. Douadi, S. Issaadi, C. Penverne, S. Chafa, Electrochemical and DFT studies of a new synthesized Schiff base as corrosion inhibitor in 1 M HCl, Measurement 99 (2017) 53−63.

[2] C. Feng, W. Qian, J. Liu, S. Han, N. Fu, F. Ye, H. Lin, J. Jiang, Effect of ultrasonication on Ni−Mo coatings produced by DC electroformation, RSC Adv. 6 (2016) 30652−30660.

[3] M.K. Das, R. Li, J. Qin, X. Zhang, K. Das, A. Thueploy, S. Limpanart, Y. Boonyongmaneerat, M. Ma, R. Liu, Effect of electrodeposition conditions on structure and mechanical properties of Ni-W/diamond composite coatings, Surf. Coating. Technol. 309 (2017) 337−343.

[4] P.C. Huang, K.H. Hou, G.L. Wang, M.L. Chen, J.R. Wang, Corrosion resistance of the Ni-Mo alloy coatings related to coating's electroplating parameters, Int. J. Electrochem. Sci. 10 (2015) 4972−4984.

[5] M.H. Allahyarzadeh, M. Aliofkhazraei, A.R. Rezvanian, V. Torabinej, A.R. Sabour Rouhaghdam, Ni-W electrodeposited coatings: characterization, properties and applications, Surf. Coating. Technol. 307 (2016) 978−1010.

[6] Y. Yang, Y. Zhang, Y. Zhang, B. Yan, F. Mo, Corrosion properties of ultrasonic electrodeposited nanocrystalline and amorphous patterned Ni−W alloy coatings, Mod. Phys. Lett. B 27 (2013), 1341007-1−1341007-7.

[7] G.S. Tasić, U. Lačnjevac, M.M. Tasić, M.M. Kaninski, V.M. Nikolić, D.L. Žugić, V.D. Jović, Influence of electrodeposition parameters of Ni-W on Ni cathode for alkaline water electrolyser, Int. J. Hydrog. Energy 38 (2013) 4291−4297.

[8] H. Wang, R. Liu, F.J. Cheng, Y. Cao, G.F. Ding, X.L. Zhao, Electrodepositing amorphous Ni-W alloys for MEMS, Microelectron. Eng. 87 (2010) 1901−1906.

[9] M. Haj-Taieb, A.S.M.A. Haseeb, J. Caulfield, K. Bade, J. Aktaa, K.J. Hemker, Thermal stability of electrodeposited LIGA Ni−W alloys for high temperature MEMS applications, Microsyst. Technol. 14 (2008) 1531−1536.

[10] T.K. Do, A. Lund, A reliability study of a new nanocrystalline nickel alloy barrier layer for electrical contacts, in: Proceedings of the 56th IEEE Holm Conference on Electrical Contacts, IEEE, 2010, pp. 1−9.

[11] E.W. Brooman, Corrosion performance of environmentally acceptable alternatives to cadmium and chromium coatings: chromium—Part II, Met. Finish. 98 (2000) 39−45.

https://doi.org/10.1016/j.heliyon.2019.e01288

[12] S. Kirihara, Y. Umeda, K. Tashiro, H. Honma, O. Takai, Development of Ni-W alloy plating as a substitution of hard chromium plating, Trans. Mater. Res. Soc. Jpn. 41 (2016) 35−39.

[13] C. Borgia, T. Scharowsky, A. Furrer, C. Solenthaler, R. Spolenak, A combinatorial study on the influence of elemental composition and heat treatment on the phase composition, microstructure and mechanical properties of Ni−W alloy thin films, Acta Mater. 59 (2011) 386−399.

[14] M. Nazarian-Samani, R. Mobarra, A.R. Kamali, M. Nazarian- Samani, Structural evolution of nanocrystalline nickel-tungsten alloys upon mechanical alloying with subsequent annealing, Metall. Mater. Trans. 45 (2014) 510−521.

[15] V. Torabinejad, M. Aliofkhazraei, A.S. Rouhaghdam, M.H. Allahyarzadeh, Electrodeposition of Ni−Fe−Mn/Al_2O_3 functionally graded nanocomposite coatings, Surf. Eng. 33 (2017) 122−130.

[16] E. Garcıa-Lecina, I. Garcıa-Urrutia, J.A. Dıez, M. Salvo, F. Smeacetto, G. Gautier, R. Seddon, R. Martin, Electrochemical preparation and characterization of Ni/SiC compositionally graded multilayered coatings, Electrochim. Acta 54 (2009) 2556−2562.

[17] X. Li, D. Zhang, Z. Liu, Z. Li, C. Du, C.F. Dong, Materials science: share corrosion data, Nature 527 (2015) 441−442.

[18] R.A. Shakoor, R. Kahraman, U.S. Waware, Y. Wang, W. Gao, Synthesis and properties of electrodeposited Ni−B−CeO_2 composite coatings, Mater. Des. 59 (2014) 421−429.

[19] L. Feng, H. Yang, F. Wang, Experimental and theoretical studies for corrosion inhibition of carbon steel by imidazoline derivative in 5% NaCl saturated $Ca(OH)_2$ solution, Electrochim. Acta 58 (2011) 427−436.

[20] S.W. Xia, M. Qiu, L.M. Yu, F.G. Liu, H.Z. Zhao, Molecular dynamics and density functional theory study on relationship between structure of imidazoline derivatives and inhibition performance, Corros. Sci. 50 (2008) 2021−2029.

[21] P.B. Raja, A.K. Qureshi, A. Abdul Rahim, H. Osman, K. Awang, Neolamarckia cadamba alkaloids as eco-friendly corrosion inhibitors for mild steel in 1 M HCl media, Corros. Sci. 69 (2013) 292−301.

[22] K.C. Emregul, M. Hayval, Studies on the effect of vanillin and protocatechualdehyde on the corrosion of steel in hydrochloric acid, Mater. Chem. Phys. 83 (2004) 209−216.

https://doi.org/10.1016/j.heliyon.2019.e01288

[23] X. Li, S. Deng, H. Fu, G. Mu, Synergistic inhibition effect of rare earth cerium(IV) ion and 3,4-dihydroxybenzaldehye on the corrosion of cold rolled steel in H_2SO_4 solution, Corros. Sci. 51 (2009) 2639−2651.

[24] P. Indyka, E.L. Beltowska, L. Tarkowskib, A. Bigosb, E. Garcia-Lecinac, Structure characterization of nanocrystalline Ni−W alloys obtained by electrodeposition, J. Alloys Comp. 590 (2014) 75−79.

[25] L. Hao, J. Wei, F.X. Gan, Electroless Ni-P coating on W-Cu composite via three different activation processes, Surf. Eng. 25 (2009) 372−375.

[26] B.D. Cullity, Elements of X-Ray Diffraction, second ed., Addison-Wesley, Reading, MA, 1978.

[27] K. Krishnaveni, T.S.N. Sankara Narayanan, S.K. Seshadri, Corrosion resistance of electrodeposited Ni−B and Ni−B−Si_3N_4 composite coatings, J. Alloy. Comp. 480 (2009) 765−770.

[28] U. Pramod Kumar, C. Joseph Kennady, Effect of benzaldehyde on the electrodeposition and corrosion properties of Ni−W alloys, Int. J. Min. Metall. Mater. 22 (2015) 1060−1066.

[29] B. Bakhita, A. Akbaria, F. Nasirpouria, M.G. Hosseini, Corrosion resistance of Ni−Co alloy and Ni−Co/SiC nanocomposite coatings electrodeposited by sediment codeposition technique, Appl. Surf. Sci. 307 (2014) 351−359.

[30] F.D. Fatah, F. Nasirpouri, A study on electrodeposition of Ni-noncovalnetly treated carbon nanotubes nanocomposite coatings with desirable mechanical and anti-corrosion properties, Surf. Coating. Technol. 248 (2014) 63−73.

[31] M.K. Awad, M.S. Metwally, S.A. Soliman, A.A. El-Zomrawy, M.A. bedair, Experimental and quantum chemical studies of the effect of poly ethylene glycol as corrosion inhibitors of aluminum surface, J. Ind. Eng. Chem. 20 (2014) 796−808.

[32] A.R. Shetty, A. Chitharanjan Hegde, Ultrasound induced multilayer Ni-Co alloy coatings for better corrosion protection, Surf. Coating. Technol. 322 (2017) 99−107.

[33] Y. Fan, Y. He, P. Luo, T. Shi, H. Li, J. Pulse current electrodeposition and characterization of Ni-W-MWCNTs nanocomposite coatings, Electrochem. Soc. 162 (2015) D270−D274.

[34] I. Danaee, S. Noori, Kinetics of the hydrogen evolution reaction on NiMn graphite modified electrode, Int. J. Hydrog. Energy 36 (2011) 12102−12111.

https://doi.org/10.1016/j.heliyon.2019.e01288

[35] S. Rashmi, L. Elias, A.C. Hegde, Multilayered Zn-Ni alloy coatings for better corrosion protection of mild steel, Eng. Sci. Technol. Int. J. 20 (2017) 1227−1232.

[36] R.K. Shervedani, A. Lasia, Studies of the hydrogen evolution reaction on Ni-P electrodes, J. Electrochem. Soc. 144 (1997) 511−519.

[37] M. Bucko, U. Lacnjevac, J. Bajat, The influence of substituted aromatic aldehydes on the electrodeposition of Zn−Mn alloy, J. Serb. Chem. Soc. 78 (2013) 1569−1581.

[38] J.N. Balaraju, V.E. Selvi, V.K.W. Grips, K.S. Rajam, Electrochemical studies on electroless ternary and quaternary Ni−P based alloys, Electrochim. Acta 52 (2006) 1064−1074.

[39] C. Liu, F. Su, J. Liang, Nanocrystalline Co-Ni alloy coating produced with supercritical carbon dioxide assisted electrodeposition with excellent wear and corrosion resistance, Surf. Coating. Technol. 292 (2016) 37−43.

[40] F. Nasirpouri, S.J. Bending, L.M. Peter, H. Fangohr, Electrodeposition and magnetic properties of three-dimensional bulk and shell nickel mesostructures, Thin Solid Films 519 (2011) 8320−8325.

[41] K.O. Nayana, T.V. Venkatesha, Effect of ethyl vanillin on ZnNi alloy electrodeposition and its properties, Bull. Mater. Sci. 37 (2014) 1137−1146.

[42] D.D. Shreeram, S. Li, V. Bedekar, H. Cong, G.L. Doll, Effect of reverse pulse time on electrodeposited Ni-W coatings, Surf. Coating. Technol. 325 (2017) 386−396.

[43] A. Brenner, Electrodeposition of Alloys, Academic Press, 1963.

[44] O. Younes, L. Zhu, Y. Rosenberg, Y. Shacham-Diamand, E. Gileadi, Electroplating of amorphous thin films of tungsten/nickel alloys, Langmuir 17 (2001) 8270−8275.

[45] K. Arunsunai Kumar, G. Paruthimal Kalaignan, V.S. Muralidharan, Pulse electrodeposition and characterization of nano Ni−W alloy deposits, Appl. Surf. Sci. 259 (2012) 231−237.

[46] A. Bahramian, M. Eyraud, F. Vacandio, P. Knauth, Improving the corrosion properties of amorphous Ni-P thin films using different additives, Surf. Coating. Technol. 345 (2018) 40−52.

[47] N. Tsyntsaru, H. Cesiulis, M. Donten, J. Sort, E. Pellicer, E.J. Podlah-Murphy, Modern trends in tungsten alloys electrodeposition with iron group metals, Surf. Eng. Appl. Electrochem. 48 (2012) 491−520.

https://doi.org/10.1016/j.heliyon.2019.e01288

[48] U. Pramod Kumar, C. Joseph Kennady, Influence of vanillin on the corrosion behavior of Ni-W alloy electrodeposits and its properties, J. Electroanal. Chem. 782 (2016) 67−75.

[49] F. Nasirpouri, M.R. Sanaeian, A.S. Samardak, E.V. Sukovatitsina, A.V. Ognev, L.A. Chebotkevich, M.G. Hosseini, M. Abdolmaleki, An investigation on the effect of surface morphology and crystalline texture on corrosion behavior, structural and magnetic properties of electrodeposited nanocrystalline nickel films, Appl. Surf. Sci. 292 (2014) 795−805.

[50] N.S. Qu, K.C. Chan, D. Zhu, Surface roughening in pulse current and pulse reverse current electroforming of nickel, Surf. Coating. Technol. 91 (1997) 220−224.

[51] M. Motoyama, Y. Fukunaka, T. Sakka, Y.H. Ogata, Electrochemical processing for Cu and Ni nanowire arrays, Electrochem. Soc. 153 (2006) 502−508.

[52] W. Schwarzacher, Kinetic roughening of electrodeposited films, J. Phys. Condens. Matter 16 (2004) 859.

[53] T. Alisina, G. Mengnan, H.H. Rotermund, The effect of surface morphology on corrosion performance of SS 316 LVM biomedical devices, JMEPEG 24 (2015) 3726−3736.

[54] W. Sassi, L. Dhouibia, P. Bercot, M. Rezrazib, E. Triki, Effect of pyridine on the electrocrystallization and corrosion behavior of Ni−W alloy coated from citrate−ammonia media, Appl. Surf. Sci. 263 (2012) 373−381.

[55] H. Timothy Gfroerer, P.L in Analysis of Surface and Interface, John Wiley & Sons, Ltd, 2006.

[56] Xuefeng Ren, Ying Song, Anmin Liu, Jie Zhang, Guohui Yuan, Peixia Yang, Jinqiu Zhang, Maozhong An, Daniel Matera, Gang Wu, Computational chemistry and electrochemical studies of adsorption behavior of organic additives during gold deposition in cyanide-free electrolytes, Electrochim. Acta 176 (2015) 10−17.

[57] A. Ehsani, M.G. Mahjani, R. Moshrefi, H. Mostaanzadeha, J.S. Shayeh, Electrochemical and DFT study on the inhibition of 316L stainless steel corrosion in acidic medium by 1-(4-nitrophenyl)-5-amino-1H-tetrazole, RSC Adv. 4 (2014) 20031−20037.

[58] S. El Issami, L. Bazzi, M. Mihit, B. Hammouti, S. Kertit, E.A. Addi, R. Salghi, Triazolic compounds as corrosion inhibitors for copper in hydrochloric acid, Pigment Resin Technol. 36 (2007) 161−168.

https://doi.org/10.1016/j.heliyon.2019.e01288

[59] K. Barouni, L. Bazzi, R. Salghi, M. Mihit, B. Hammouti, A. Albourine, S. El Issami, Some amino acids as corrosion inhibitors for copper in nitric acid solution, Mater. Lett. 62 (2008) 3325−3327.

[60] M.K. Awad, Semiempirical investigation of the inhibition efficiency of thiourea derivatives as corrosion inhibitors, J. Electroanal. Chem. 567 (2004) 219−225.

[61] J. Zhang, G. Qiao, S. Hu, Y. Yan, Z. Ren, L. Yu, Theoretical evaluation of corrosion inhibition performance of imidazoline compounds with different hydrophilic groups, Corros. Sci. 53 (2011) 147−152.

https://doi.org/10.1016/j.heliyon.2019.e01288